AIP | Journal of Applied Physics

Performance of perpendicular magnetic recording with track squeeze using bidirectional pattern-dependent noise prediction detector

Yibin Ng, Songhua Zhang, Kui Cai, Zhiliang Qin, Chun Lian Ong, Shiming Ang, and Zhi-Min Yuan

Citation: Journal of Applied Physics **117**, 17E315 (2015); doi: 10.1063/1.4913899
View online: http://dx.doi.org/10.1063/1.4913899
View Table of Contents: http://scitation.aip.org/content/aip/journal/jap/117/17?ver=pdfcov
Published by the AIP Publishing

Performance of perpendicular magnetic recording with track squeeze using bidirectional pattern-dependent noise prediction detector

Yibin Ng,[a] Songhua Zhang, Kui Cai, Zhiliang Qin, Chun Lian Ong, Shiming Ang, and Zhi-Min Yuan
*Data Storage Institute, Agency for Science, Technology and Research (A*STAR), Singapore 117608*

(Presented 6 November 2014; received 16 September 2014; accepted 28 October 2014; published online 18 March 2015)

In this study, we investigated the performance of perpendicular magnetic recording with squeezed tracks. Based on spinstand signals, we developed a signal generation module to generate the readback signals for tracks of various squeezed track width and bit length. To mitigate the drop in bit error rate (BER) as squeezed track width decreases, we implemented the bidirectional pattern-dependent noise prediction (BiPDNP) detector with low-density parity check codes. To improve the BiPDNP detector over earlier work, we modified the log-likelihood ratio computation. Our results show that our proposed BiPDNP detector improves the bit error rate, and allows smaller squeezed track width and smaller bit length for the same BER performance. © *2015 AIP Publishing LLC*.
[http://dx.doi.org/10.1063/1.4913899]

I. INTRODUCTION

Shingled magnetic recording (SMR) has been widely recognized as a promising technology that can extend the storage density of magnetic storage systems beyond 1 Tb/in^2.[1] Shingled writing is advantageous because it allows a strong head field using a wide main-pole with a large track width.[2] Other advantages of shingled writing include increase in track density by allowing adjacent tracks to overlap each other, as well as larger off-track capability over conventional writing for the same track pitch.[2] However, this results in an increase in electronics noise, transition noise, non-transition noise, and inter-track interference power as the track pitch decreases.[3] There is a need for novel and improved detectors to combat these effects.

In this paper, we developed a signal model for perpendicular recording with squeezed tracks using signals obtained from the spinstand. Compared to channel models based solely on simulations, using actual spinstand signals to develop our channel model give us more realistic results. Although we can directly perform signal processing on the spinstand signals and obtain the raw bit error rate (BER), this approach is not practical when we choose to evaluate the BER after error correction coding (ECC). To obtain the BER results after ECC, a large quantity of data sectors which are not obtainable from spinstand testing are required. Therefore, in this work readback signals for squeezed tracks are first obtained from the spinstand, after which a signal generation module is developed based on these spinstand signals. This signal generation module is then used to generate the readback signals to obtain the BER results after signal processing and ECC.

In our earlier work, we proposed the bidirectional pattern-dependent noise prediction (BiPDNP) detector to combat the high jitter noise problem.[4,5] The main idea in BiPDNP is to utilize both forward and backward linear prediction to predict the noise samples.[4] When low-density parity check (LDPC) codes are included, we averaged the *a posteriori* probabilities (APPs) from the Bahl-Cocke-Jelinek-Raviv (BCJR) detectors employing forward and backward PDNP to obtain more accurate soft information.[5]

In this work, we applied the BCJR detector incorporated with BiPDNP and LDPC code on perpendicular recording with squeezed tracks. Further, we improved our BiPDNP detector by combining the log-likelihood ratios (LLRs) instead of averaging the APPs. We found that this gives better BER performance. The performance improvement of BiPDNP over conventional PDNP is evaluated.

II. CHANNEL MODELING

Unlike conventional magnetic recording where the recorded track is defined with a single pass of the writing head leaving erasure band in between neighboring tracks, in shingled recording the recorded track is finalized by partial erasure when writing the neighboring track. It therefore reuses the low signal-to-noise ratio (SNR) guard-band to increase overall track density. However, with such a novel setup, the channel model of squeezed track needs to be carefully studied so that optimum channel detector can be developed. In this study, we conducted track squeezing on spinstand to get the readback signal of both periodic and pseudo-random datasets from which we characterize the various channel parameters such as jitter distribution, media noise, and pattern dependent transition shifts for different squeezed track width. Such analysis can assist in optimizing the choices of recording parameters such as bit-aspect ratio (BAR) to maximize the overall recording density. In this section, we describe in detail the following components in our characterized signal.

In conventional recording, due to the circular shape of the write field, the magnetization transitions recorded on media assume certain curvature, which in turn produce an S-curve transition response as read sensor response. In Fig. 1,

[a]Electronic mail: ng_yibin@dsi.a-star.edu.sg

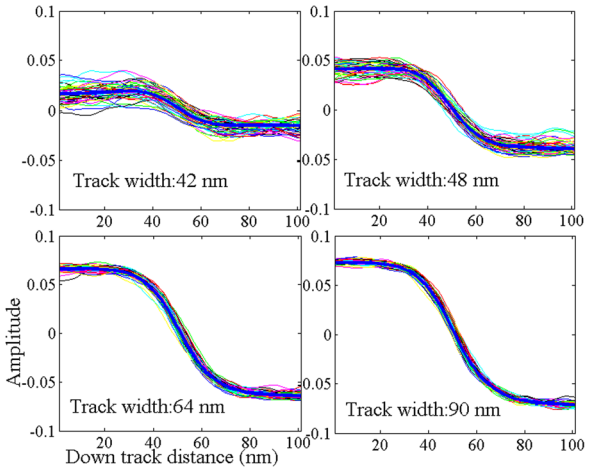

FIG. 1. Comparison of transition response for various squeezed track width: bold blue curve is the average transition response, while the more random thin curve represents individual transitions that contain jitter and noise.

we compared the averaged transition response obtained from averaging many individual randomized transitions. The experiments are done on 2.5 in. commercial media with recording density of 500 GB/platter. The writer used to conduct the track squeezing operation has a width of around 65 nm. The reader width is around 43 nm. Two observations are notable here: (1) as the tracks are being squeezed narrower, its amplitude decreases accordingly and the jitter noise spread becomes larger and (2) the transition appears to be sharper for narrower track due to the magnetization curvature reduction caused by erasure of track edge.

Transition jitters remain a major concern in high density magnetic recording. As bit size shrinks there are fewer grains per bit causing higher random transition jitter. On top of that shorter bit length causes higher data pattern dependent transition shift. Another noticeable signal distortion is a low frequency amplitude drift. It can be described by a DC level drift and envelope (peak-to-peak) variation. Fig. 2 summarizes the separated noise level due to jitter and dc drift for different squeezed track width. The results suggest that the signal quality only starts to deteriorate after track width is squeezed below 60 nm. Here, for the purpose of reducing inter-symbol-interference in estimating saturated transition response the recording transition frequency is chosen to be only 200 kilo flux change per inch (KFCI), much lower than data recording frequency, actual jitter percentage observed in data channel shall be scale up 5–10 times for the prevailing 1–2 mega flux change per inch recording frequency.

In our analysis of the signal characteristics, after reconstructing a signal waveform with averaged transition response, adding random and pattern-dependent transition jitter and DC/envelope modulation, we observe a colored residual noise with typical spectrum shown in Fig. 3. We believe this data pattern independent noise is the combination of media noise and thermal noise.

The above signal characterization results enable us to build a channel simulator that generate readback signals from arbitrary input data pattern with accurate statistics for the various noise sources with different squeezed track width. With this, we can test and optimize our proposed BiPDNP detector to achieve maximized areal density for a given head/media setup.

III. BIDIRECTIONAL PATTERN-DEPENDENT NOISE PREDICTION DETECTOR

After developing the signal generator module for perpendicular recording with squeezed tracks, next, we develop the channel detector. PDNP is a near-maximum likelihood sequence detection (MLSD) scheme for zero-mean, data-dependent, and finite-memory Gauss-Markov noise.[6] To implement PDNP, we denote the equalized channel output as

$$y_k = s_k\left(a_{k-M_1}^{k+\Delta_1}\right) + n_k\left(a_{k-M}^{k+\Delta}\right), \tag{1}$$

where s_k and n_k are the desired signal component and noise component, respectively. The data-dependence of s_k are made explicit in (1), where $a_{k-M_1}^{k+\Delta_1}$ is a shorthand notation for the sequence $\{a_{k-M_1}, \ldots, a_{k+\Delta_1}\}$. Unlike the previous work, where s_k is computed analytically from the target coefficients,[4,5] s_k is computed using the training sequence, by taking the average of all the y_k components corresponding to the data pattern $a_{k-M_1}^{k+\Delta_1}$. In doing so, we ensure that reader asymmetry effects are taken care of in s_k, and n_k is effectively zero-mean. The choice of the data-dependent lengths in (1) results in our detector trellis having $2^{\max(\Delta_1,\Delta)+\max(M_1+L,M)}$ states.

We incorporate the PDNP scheme[6] into the BCJR algorithm[7] to obtain the APP of the detected bit $\Pr(a_k|\underline{y})$, where

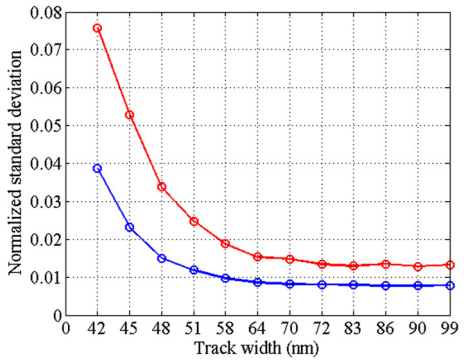

FIG. 2. Standard deviation of jitter (normalized to bit length) and DC drift (normalized to average transition peak-to-peak).

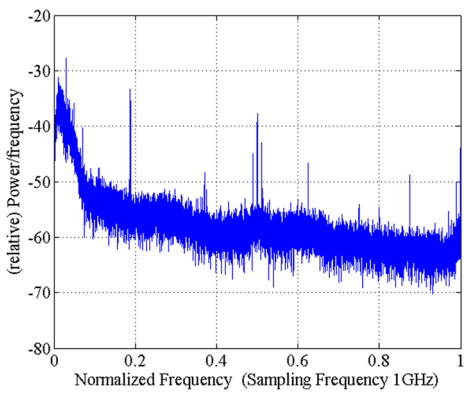

FIG. 3. Spectrum of residual noise after removing jitter noise, DC drift, and envelope modulation.

$a_k \epsilon \{+1, -1\}$ denotes the data input and $\underline{y}$ denotes the detector input sequence. Denote S_k as the trellis state at time instant k, and m', m, and m'' as the past, current, and future states of the trellis. To implement the BCJR algorithm, we compute the joint probability density function (p.d.f.) $f(a_k, \underline{y})$. So we have

$$f(a_k, \underline{y}) = \sum_{m'} \alpha_{k-1}(m') \cdot \gamma_k(m', m) \cdot \beta_k(m), \tag{2}$$

where

$$\alpha_{k-1}(m') = f(S_{k-1} = m', y_0^{k-1}), \tag{3}$$

$$\beta_k(m) = f(y_{k+1}^{N-1} | S_k = m), \tag{4}$$

and

$$\gamma_k(m', m) = f(y_k | S_{k-1} = m', S_k = m) \cdot \Pr(a_k). \tag{5}$$

The variables $\alpha_k(m)$ and $\beta_k(m)$ can be computed recursively using

$$\alpha_k(m) = \sum_{m'} \alpha_{k-1}(m') \cdot \gamma_k(m', m), \tag{6}$$

and

$$\beta_k(m) = \sum_{m''} \beta_{k+1}(m'') \cdot \gamma_{k+1}(m, m''). \tag{7}$$

In the log domain, the computation on each branch with PDNP is given by

$$\gamma_k(m', m) = a_k L_{in}(a_k)/2 - \ln\sigma_p\left(a_{k-M}^{k+\Delta}\right) - \frac{\left[y_k - \hat{n}_k\left(a_{k-M}^{k+\Delta}\right) - s_k\left(a_{k-M_1}^{k+\Delta_1}\right)\right]^2}{2\sigma_p^2\left(a_{k-M}^{k+\Delta}\right)}, \tag{8}$$

where $L_{\text{in}}(a_k) = \ln(\Pr(a_k = +1)/\Pr(a_k = -1))$ is the extrinsic information obtained from the LDPC decoder and $\sigma_p^2(a_{k-M}^{k+\Delta})$ is the predictor error variance. The predicted noise sample $\hat{n}_k$ is computed using

$$\hat{n}_k(a_{k-M}^{k+\Delta}) = \sum_{i=1}^{L} f_i\left(a_{k-M}^{k+\Delta}\right) n_{k-i}\left(a_{k-i-M_1}^{k-i+\Delta_1}\right) = \sum_{i=1}^{L} f_i\left(a_{k-M}^{k+\Delta}\right)\left[y_{k-i} - s_{k-i}\left(a_{k-i-M_1}^{k-i+\Delta_1}\right)\right], \tag{9}$$

where f_i denotes the noise predictor coefficients and L is the length of the predictor. Further, the predictor error variance σ_p^2 is defined as

$$\sigma_p^2\left(a_{k-M}^{k+\Delta}\right) = E\left\{(n_k - \hat{n}_k)^2 | a_{k-M}^{k+\Delta}\right\}. \tag{10}$$

Here, f_i and σ_p^2 can be computed from the data-dependent noise covariance matrix.[4]

Backward PDNP can be incorporated into the BCJR algorithm by time-reversing the input into the BCJR detector. In doing so, the predicted noise sample $\hat{n}_k$ is computed using

$$\hat{n}_k\left(a_{k-\Delta^b}^{k+M^b}\right) = \sum_{i=1}^{L^b} b_i\left(a_{k-\Delta^b}^{k+M^b}\right) n_{k+i}\left(a_{k+i-\Delta_1^b}^{k+i+M_1^b}\right) = \sum_{i=1}^{L^b} b_i\left(a_{k-\Delta^b}^{k+M^b}\right)\left[y_{k+i} - s_{k+i}\left(a_{k+i-\Delta_1^b}^{k+i+M_1^b}\right)\right], \tag{11}$$

where b_i denotes the backward noise predictor. In the above, we denote the backward PDNP parameters to be Δ^b, $\Delta_1{}^b$, M^b, $M_1{}^b$, and L^b to indicate that they need not be the same as the forward PDNP parameters.

In the previous work,[5] we averaged the APPs of the forward and backward PDNP to obtain a more accurate LLR. Denoting the APP of BCJR with backward PDNP as $\Pr(a_k|\underline{y}^b)$, the LLR input to the LDPC decoder is given by

$$LLR = \ln\frac{\Pr(a_k = +1|\underline{y}) + \Pr\left(a_k = +1|\underline{y}^b\right)}{\Pr(a_k = -1|\underline{y}) + \Pr\left(a_k = -1|\underline{y}^b\right)}. \tag{12}$$

However, subsequently, we found that averaging the LLRs instead of the APPs give better BER results. In this work, the LLR input to the LDPC decoder is computed as

$$LLR = \alpha(LLR^{(f)} + LLR^{(b)}), \tag{13}$$

where $LLR^{(b)}$ denotes the LLR from the BCJR with backward PDNP. Here, $\alpha \epsilon (0,1]$ denotes a normalization factor, which is to be optimized at each squeezed track width and bit length values for better performance. We call this the combined LLR method.

Fig. 4 shows the model of BiPDNP with LDPC code using the combined LLR method. Data bits are encoded in the LDPC encoder and passed into the channel model described in Sec. II. The readback signal is then passed into two different equalizers with different targets. Equalizer 1 denotes the conventional equalizer with monic constraint set at the first tap of the target. Equalizer 2 denotes the equalizer for backward PDNP, where the monic constraint is set at the last tap of the target. For BiPDNP, using two equalizers will obtain better BER results than using a single equalizer.[4] The output of equalizer 1 is passed into BCJR incorporated with forward PDNP as described earlier. Similarly, the output of equalizer 2 is passed into BCJR with backward PDNP. The outputs of the two BCJR detectors are combined using (13),

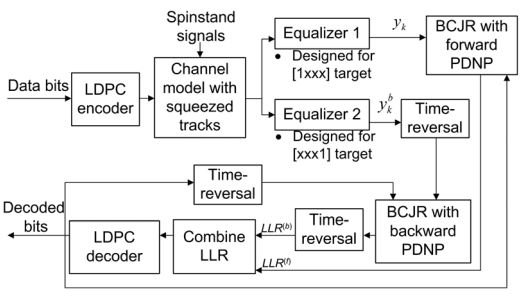

FIG. 4. Discrete-time model of BiPDNP with LDPC code using the combined LLR method.

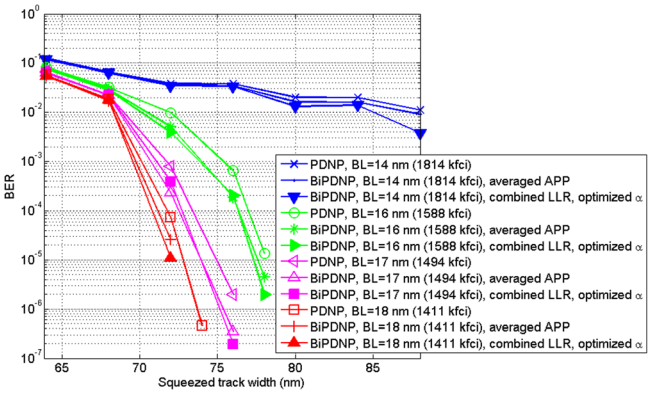

FIG. 5. BER versus squeezed track width with varying linear density.

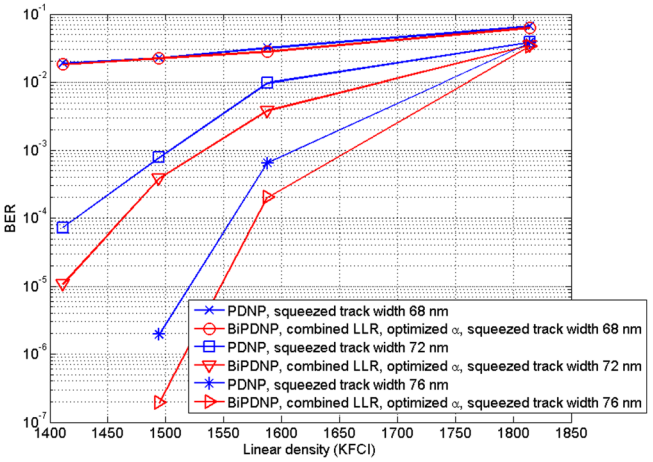

FIG. 6. BER versus linear density with varying squeezed track width.

and then LDPC decoding is performed. Finally, extrinsic information at the output of the LDPC decoder is passed back to the BCJR detectors to perform turbo equalization.

IV. EMULATION RESULTS

For the emulations, we used generalized partial-response (GPR) equalizers.[8] The equalizer length is arbitrarily chosen to be 51 to ensure small mis-equalization noise. The LDPC code used here is a (4096, 3841) random LDPC code based on the progressive-edge growth (PEG) algorithm with code rate $R = 0.938$ and column weight of 4. Iterative processing is performed to achieve a higher coding gain. In the simulations, the number of turbo iterations between the BCJR detector and the LDPC decoder is set to 3, and the maximum number of sum-product decoding iterations within the LDPC decoder per turbo iteration is set to 30. All our results below include the LDPC code. For example, when we show BER results for "PDNP," we mean BER results obtained at the output of the BCJR detector incorporated with conventional forward PDNP, followed by the LDPC decoder.

Fig. 5 plots BER against squeezed track width, in the range of 64–88 nm. Here, the bit length is varied between 14, 16, 17, and 18 nm. It can be observed that BiPDNP with combined LLR and optimized α achieves a superior performance over BiPDNP using averaged APPs proposed in our earlier work.[5] The detrimental effects of decreasing squeezed track width and bit length are easily observed. The use of BiPDNP is able to help mitigate these detrimental effects. At squeezed track width greater than 72 nm and bit length greater than 16 nm, BiPDNP achieves a superior performance improvement over conventional PDNP. At a given bit length and BER, the use of BiPDNP allows a smaller squeezed track width compared to conventional PDNP.

Fig. 6 plots BER against linear density, in the range of 1411–1814 KFCI. Here, the squeezed track width is varied between 68, 72, and 76 nm. Once again it can be observed that BiPDNP offers a superior performance improvement over conventional forward PDNP. For example, at linear density 1494 KFCI, as squeezed track width decreases from 76 to 72 nm, the BER increases from 2×10^{-6} to 8×10^{-4} if conventional PDNP is used. However, if the BiPDNP detector is used, the BER is increased only to 4×10^{-4}. Therefore, the use of the BiPDNP detector allows for narrower squeezed track width compared to conventional PDNP. As another example, at squeezed track width 76 nm and 1494 KFCI, BiPDNP (at BER 2×10^{-7}) offers one order of magnitude performance improvement over conventional PDNP (at BER 2×10^{-6}). Also, at a given squeezed track width and BER, the use of BiPDNP allows higher linear densities for the same BER performance.

V. CONCLUSION

In this work, we evaluated the performance of the BiPDNP detector for perpendicular magnetic recording with squeezed tracks. To generate the readback signals with various squeezed track width, we developed an emulation model using actual spinstand signals. Our BER results show that the proposed BiPDNP detector will be helpful in improving the BER performance at squeezed track width greater than or equal to 72 nm and bit lengths greater than 16 nm. Further, our BiPDNP detector allows for smaller squeezed track width and higher linear densities compared to conventional PDNP.

[1]R. Wood *et al.*, IEEE Trans. Magn. **45**, 917 (2009).
[2]K. Miura *et al.*, IEEE Trans. Magn. **45**, 3722 (2009).
[3]R. Galbraith *et al.*, IEEE Trans. Magn. **50**, 3200707 (2014).
[4]Y. Ng *et al.*, IEEE Trans. Magn. **48**, 1819 (2012).
[5]Y. Ng *et al.*, IEEE Trans. Magn. **49**, 2661 (2013).
[6]J. Moon *et al.*, IEEE J. Sel. Areas Commun. **19**, 730 (2001).
[7]L. R. Bahl *et al.*, IEEE Trans. Inf. Theory **20**, 284 (1974).
[8]J. Moon *et al.*, IEEE Trans. Magn. **31**, 1083 (1995).